X-ray Absorption Spectroscopic Investigation of Partially Reduced Cobalt Species in Co−MCM-41 Catalysts during Synthesis of Single-Wall Carbon Nanotubes

Dragos Ciuparu,*,† Peter Haider,‡ Marcos Fernández-García,§ Yuan Chen,† Sangyun Lim,† Gary L. Haller,† and Lisa Pfefferle†

Department of Chemical Engineering, Yale University, P.O. Box 208286, New Haven, Connecticut, Department Chemie, Lehrstuhl für Technische Chemie II, TU München, Germany, and Instituto de Catálisis y Petroleoquímica, CSIC, 28049-Madrid, Spain

Received: April 29, 2005; In Final Form: June 29, 2005

Chemometric tools were employed to analyze the in-situ dynamic X-ray absorption spectroscopy data to probe the state of Co−MCM-41 catalysts during reduction in pure hydrogen and under single-wall carbon nanotube synthesis reaction conditions. The use of the progressive correlation analysis established the sequence in which changes in the spectral features near the Co K edge occurred, and the evolving factor analysis provided evidence for the formation of an intermediate Co^{1+} ionic species during reduction of the Co−MCM-41 catalyst in pure hydrogen up to 720 °C. This intermediate species preserves the tetrahedral environment in the silica framework and is resistant to complete reduction to the metal in H_2. While the Co^{2+} species is resistant to reduction in pure CO, the intermediate Co^{1+} species is more reactive in CO most likely forming cobalt carbonyl-like compounds with high mobility in the MCM-41. These mobile species are the precursors of the metallic clusters growing carbon nanotubes. Controlling the rates of each step of this two-stage reduction process is key to controlling the size of the metallic Co clusters formed in Co−MCM-41 catalysts.

Introduction

Synthesis of small, size-controllable metallic clusters dispersed on solid oxides is of crucial importance for catalytic applications. The thermal stability of such uniform size distribution metallic particles is also highly desirable in commercial catalysts. Mesoporous molecular sieves[1,2] and more precisely incorporation of different transition metals such as Mn,[3] Co,[4,5] Ni,[6] Fe,[7] Cr,[8] Cu,[9] Rh,[10] and so forth into their silica framework have recently received a great deal of attention. In our recent investigations of the growth of single-wall carbon nanotubes (SWNT) by CO disproportionation on Co−MCM-41 catalysts, we observed that small, stable metallic cobalt clusters of approximately 20−30 atoms can be formed by controlled reduction of the cobalt ions isomorphously substituted for silicon ions in the silica framework of the MCM-41 mesoporous molecular sieve.[11] The reducibility of the cobalt ions incorporated in the MCM-41 was found to correlate with the pore radius of curvature,[12] and the size of the metallic cobalt clusters formed under reaction conditions was observed to be sensitive to the catalyst prereduction and nanotube growth reaction conditions.[13,14] In a recent X-ray absorption spectroscopic (XAS) study of the mechanism controlling the size of the metallic cobalt clusters formed by Co−MCM-41 reduction, we observed that the prereduction treatment in hydrogen at temperatures below 700 °C increases the density of electrons at the Fermi level of the oxidized cobalt species preserving their local tetrahedral environment, and only subsequent exposure of the prereduced catalyst to CO at 750 °C produces completely reduced cobalt clusters.[15] Subsequently, using the progressive 2D correlation analysis (ProCorA), we were able to observe that the increase in the density of the occupied states at the Fermi level of the cobalt species during prereduction is accompanied by a decrease in the oxidation state of the cobalt species illustrated by the shift of the threshold of the absorption edge toward lower energy values.[16] These preliminary observations suggest that there might be an intermediate, partially reduced state of the cobalt in the silica framework of the MCM-41 molecular sieve and that this state of cobalt may play an important role in stabilizing the small metallic clusters of cobalt formed at the incipient stage of reduction by acting as anchor sites, as discussed in more detail elsewhere.[12]

The purpose of this study is twofold. First, we wish to identify and characterize the intermediary reduced cobalt state. Second, we characterize its behavior under different reducing reaction conditions aiming to better control the process of synthesizing uniform small metallic clusters by reduction of metal-incorporated MCM-41 mesoporous molecular sieves.

Experimental Section

The Co−MCM-41 catalysts used in these studies had 1 wt % cobalt loading (as determined by ICP-MS at Galbraith Laboratories). A C16 organic template and high-purity Cab-O-Sil fumed silica source from Cabot Corporation were used for their synthesis. The pH was carefully controlled at 11.5 during the initial stage of the synthesis because the pH was observed to strongly affect the reducibility of cobalt in the silica framework.[17] The catalyst obtained after calcination had an average pore diameter of 28.5 ± 1 Å as determined from nitrogen physisorption measurements using the BJH method.[18] The nitrogen adsorption−desorption isotherms were measured

* Author to whom correspondence should be addressed.
† Yale University.
‡ Lehrstuhl für Technische Chemie II.
§ Instituto de Catálisis y Petroleoquímica.

10.1021/jp052243p CCC: $30.25
Published on Web 08/09/2005

at −196 °C in a static volumetric instrument Autosorb-1C (Quantachrome).

The state of the Co−MCM-41 catalyst was monitored using the X-ray absorption spectra collected at beam lines X23A2 and X11B at the National Synchrotron Light Source, Brookhaven National Laboratory. X-ray absorption near-edge structure (XANES) spectra were recorded in situ both during catalyst reduction by hydrogen from room temperature to 720 °C, and during 1 h exposure to pure CO at different pressures and 750 °C after prereduction under flowing hydrogen at 500 °C for 30 min. After prereduction in hydrogen at 500 °C, the catalyst was heated to 750 °C in flowing helium. For these experiments, an 80-mg sample of fresh Co−MCM-41 was pressed at ∼5 tons into a round self-supporting wafer (1.5 cm in diameter) using a hydraulic pellet press. Wafers having an absorbance of approximately 2 were placed in the in-situ stainless-steel reaction chamber described elsewhere.[15] The XANES spectra were collected from 30 eV below to 50 eV above the Co K edge in 1 eV steps, averaging approximately 4 min per scan.

Because of the short-energy range scanned for the in-situ XANES spectra, the postedge background of the XANES spectra was not long enough to obtain an accurate edge energy jump at E_0. To compare the XANES features observed in different experiments, assuming a constant Co atom concentration under the X-ray beam (1 × 5 mm) during reaction, we used the energy edge step measured from the extended X-ray absorption fine structure (EXAFS) spectrum of the same sample recorded after each in-situ reaction XANES series. The normalized XANES spectra for each series of in-situ experiments were obtained by subtracting the fixed edge step determined from the analysis of the final EXAFS spectrum. Analysis of the EXAFS spectra followed the procedures described in detail in our previous reports.[13,15] The EXAFS spectra were calibrated to the edge energy of the cobalt foil reference. The background removal and edge-step normalization were performed using the FEFFIT code.[19] The theoretical EXAFS functions for different cobalt species (Co, Co_3O_4) generated by the FEFF6 program[20] were used to fit the experimental data to obtain the corresponding Co−Co and Co−O first-shell coordination numbers.

Results

A first experiment was designed to observe the dynamics of the cobalt species in the MCM-41 framework during catalyst reduction in hydrogen. A catalyst pellet weighing 80 mg was placed in the reaction cell and was heated in flowing hydrogen at approximately 20 °C/min to 720 °C. XANES spectra were continuously recorded during catalyst heating and isothermal reduction in flowing hydrogen at 720 °C. After 1 h at 720 °C in flowing hydrogen, the reaction cell was cooled to room temperature in approximately 15 min. The EXAFS spectrum was recorded at room temperature to determine an accurate edge energy jump at E_0 for the normalization of the XANES spectra. The series of in-situ XANES spectra recorded during this process is given in Figure 1.

Using the progressive 2D correlation analysis (ProCorA)[16] for the data in Figure 1, we have obtained the corresponding synchronous and asynchronous correlation intensities. In brief, the synchronous spectrum reveals the simultaneous changes of spectral intensity variations measured at two energy values, E_1 and E_2, by showing auto peaks of coordinates (E_1, E_1) and (E_2, E_2) located on the diagonal line in the contour plot obtained for the synchronous intensity, while the asynchronous spectrum is antisymmetric with respect to the diagonal line and develops cross-peaks only if the intensities of two spectral features change

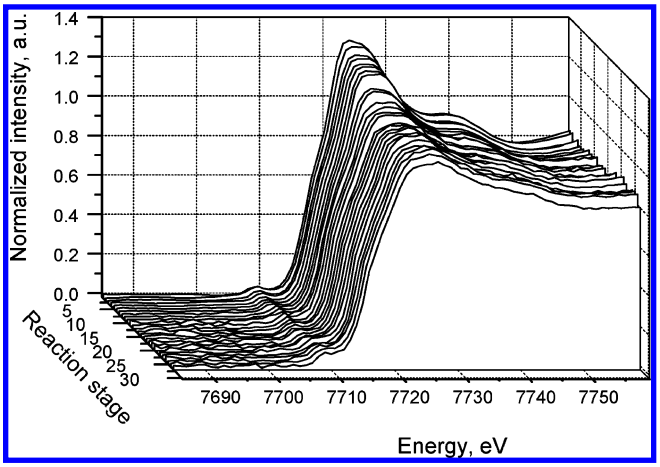

Figure 1. X-ray absorption spectra recorded in situ during Co−MCM-41 reduction with pure H_2.

out-of-phase with each other (i.e., delayed or accelerated).[21] The asynchronous spectrum has been proven instrumental in differentiating overlapped bands arising from spectral features of different origins, whose changes occur in a time sequence. Details of this analysis are given in refs 16 and 22 and references therein.

In Figure 2 are depicted for exemplification the correlation intensities obtained for the first nine spectra in the series. According to the interpretation rules established by Noda,[21,23] while the sign of the auto peaks in the synchronous plot is always positive, the sign of their corresponding cross-peaks can be either positive or negative, depending on whether the simultaneous changes are in the same direction or in opposite directions. If the intensities at the two different energies increase or decrease simultaneously, the cross-peaks will be positive, otherwise, they will be negative. The sign of an asynchronous cross-peak is positive if the intensity change at energy E_1 (with $E_1 > E_2$) occurs prior to the change of intensity at E_2 in the sequence of spectra. However, if the sign of the corresponding synchronous cross-peak intensity is negative, this rule is reversed. Applying these interpretation rules, the results in Figure 2 indicate that there are three spectral features changing in this data set, centered at approximately 7710, 7716, and 7724 eV. These spectral features were assigned to changes in the preedge peak, in the location of the threshold of the absorption edge, and in the intensity of the white line.[16] The features of the asynchronous correlation intensity and the evolution of synchronous plot during ProCorA indicated that the white line intensity decreases initially without any change in the other two spectral features suggesting an increase in the density of occupied states at the Fermi level for the oxidized cobalt species incorporated in the silica framework of the MCM-41 molecular sieve. In fact, when the first three spectra in the series were used in the ProCorA, the decrease in the intensity of the white line was accompanied by a shift of the threshold of the absorption edge toward lower energy values indicating a change in the formal oxidation state of the cobalt species, thus suggesting a partial reduction of the Co^{2+} ions. Only after the ninth spectrum was added to the series analyzed by ProCorA did the preedge feature also begin to change, indicative of changes in the local symmetry of the cobalt species in the MCM-41 silica framework.

The Fourier transforms (FTs) of the EXAFS spectrum in Figure 3 recorded at room temperature with the catalyst after the reduction experiment producing the spectra in Figure 1 give clear evidence for the presence of two cobalt species in the

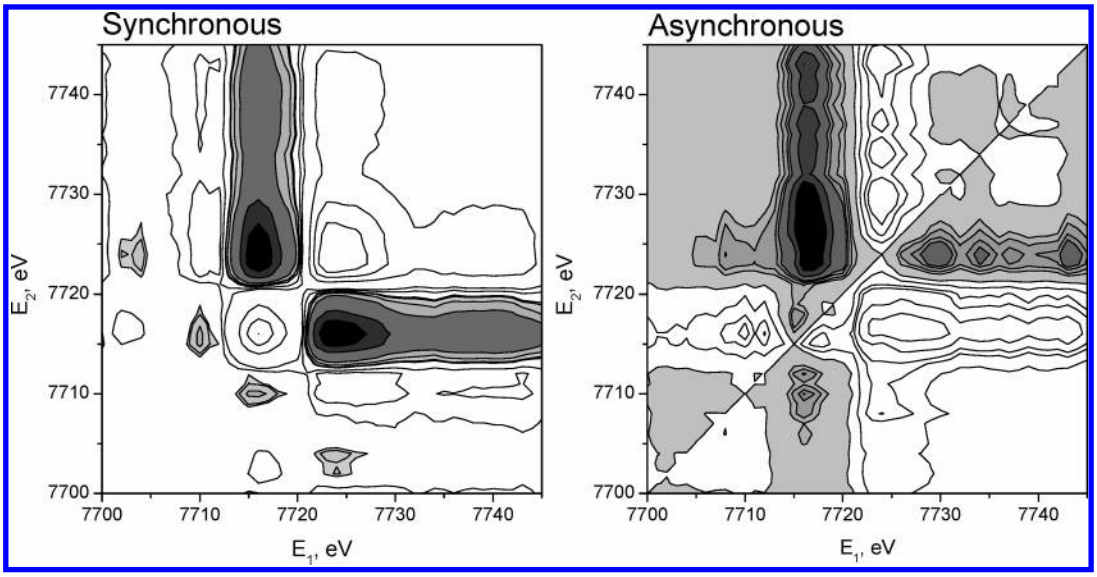

Figure 2. Synchronous (left) and asynchronous (right) correlation intensities determined with the first nine XANES spectra in Figure 1. Gray hues correspond to regions with negative intensity values.

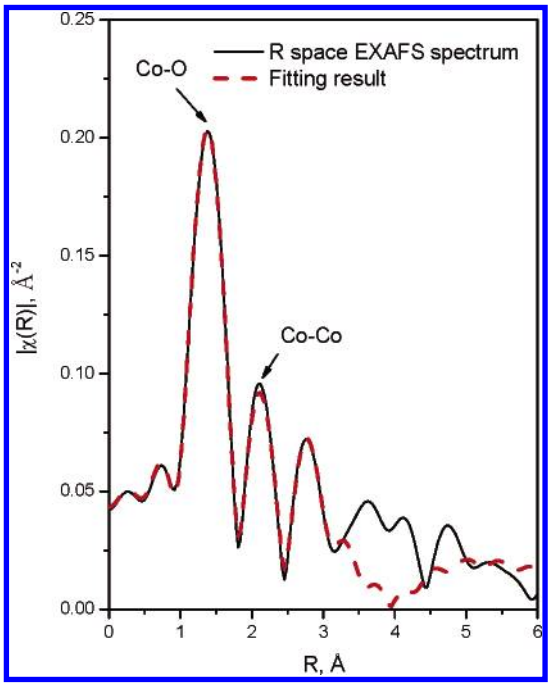

Figure 3. Fourier transforms of EXAFS spectrum recorded with the Co−MCM-41 catalyst after reduction in pure H_2 between room temperature and 720 °C and the corresponding fitting results (dotted line).

catalyst after reduction. The peak centered at approximately 1.5 Å corresponds to a Co−O bond, while the second peak at 2.2 Å is assigned to a Co−Co bond, characteristic of the development of metal−metal bonds for cobalt in a zerovalent state. The weak intensity of the Co−Co peak compared to the Co−O peak indicates that a rather small fraction of the cobalt in the catalyst was completely reduced and nucleated into small metallic cobalt clusters, as suggested by the near zero Co−Co coordination number resulting from fitting. However, application of EXAFS to determine the size of finely dispersed clusters is limited by the insensitivity of this technique to polydispersity as discussed in detail elsewhere.[24] Moreover, when the cobalt exists in two oxidation states, the coordination number determined from fitting should be corrected for the fraction of the reduced cobalt in the sample, as the EXAFS spectrum is a volume average of all the cobalt species, reduced and oxidized, in the sample. Therefore, in this case, the actual Co−Co coordination number is most likely larger than that determined from fitting and thus is only considered as a very rough, qualitative measure for the size of the cobalt clusters formed in the sample.

Chemometric tools have been previously applied to identify intermediate species from a dynamic series of spectra. Among these, the principal component analysis (PCA)[25,26] and the evolving factor analysis (EFA)[27,28] are the most commonly used in XAS data analysis. The goal of PCA is the determination of the number N of components or factors in the data set which corresponds to the rank of the data matrix used in the analysis. In the EFA, a rank analysis is performed r times, with r being the number of spectra in the data set, adding one spectrum at every step. In an evolutionary process, when a new chemical species appears, an eigenvalue evolves from the pool of noise eigenvalues, increasing in value in relation to its contribution to the enlarged data set. This analysis is performed in forward and backward mode, that is, starting with the first or the r^{th} spectrum. The calculation of both modes, forward and backward, has a unique concentration profile as a result: the j^{th} forward curve is merged with the $(r + 1 - j)^{th}$ backward curve, the smaller of the two corresponding eigenvalues always being retained.[28]

To determine the total number of cobalt species in the sample during reduction, we have first calculated the eigenvalues and their respective variance and then the reduced eigenvalues ratio (REVR) and the percentage of significance level (%SL) for the F-test. Subsequently, EFA[27] was used to determine the number of components (Figure 4). The EFA clearly evidences the existence of two species and suggests the presence of a third species in the sample. However, the level of noise created by the inherent normalization uncertainty is not clearly separated in the diagram, most likely because the concentration of each of the species is not high enough to produce a distinct cut. To obtain a better separation of the eigenvalues corresponding to real species in the samples from the level of noise, a data set recorded in situ during the complete transformation from fully oxidized Co^{2+} to fully reduced Co^0 is desirable. This would provide the basic spectra for species known to be in the sample (the starting, fully oxidized Co^{2+} species and the fully reduced

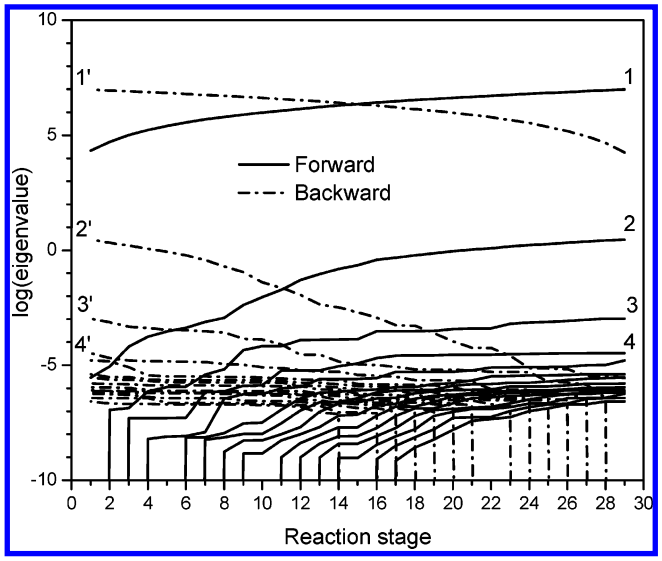

Figure 4. The EFA diagram for the data set in Figure 1: lines are for the forward (solid) and backward (dotted) analyses.

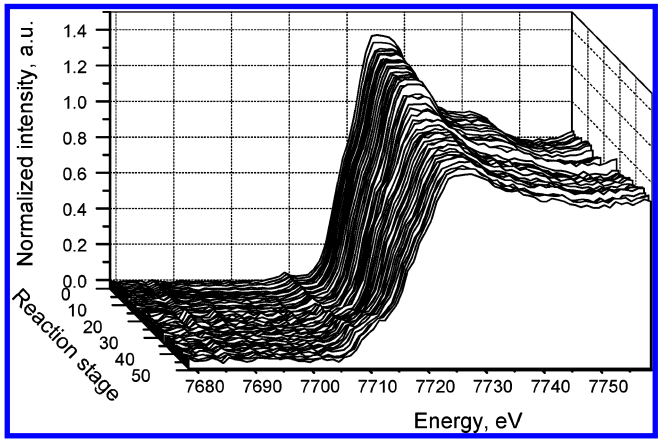

Figure 5. X-ray absorption XANES spectra recorded in situ during catalyst prereduction in H_2 and SWNT synthesis at 750 °C under 6 atm CO pressure.

metallic Co clusters). Therefore, in a separate SWNT synthesis experiment, a fresh Co−MCM-41 sample was placed in the in-situ cell, was heated at 10 °C/min in 1 atm hydrogen from room temperature to 500 °C, and was maintained for 30 min at this temperature. Then, the reaction chamber was purged with He and was heated in flowing He at 10 °C/min to 750 °C. After the temperature stabilized at 750 °C, pure CO was admitted to the cell at 6 atm total pressure, and the cell was maintained at these reaction conditions for 60 min. The XANES spectra recorded continuously during this treatment are shown in Figure 5. In previous studies, this treatment was shown to produce small metallic clusters.[12,13,15] Here, the noise level is better defined and approached −3.5 in the plot of Figure 6, for example, the limiting value reached by the fourth and subsequent eigenvalues. The EFA diagram in Figure 6 obtained with this data set confirms the presence of three principal components in this data set, consistent with the results obtained with the data set in Figure 1. The plot depicted here clearly evidences the existence of two species during H_2 prereduction at 500 °C and heating in He to 750 °C during steps 1−27. The evolution of a third species that can be clearly observed at reaction stage 28 corresponds to the beginning of the admission of CO to the reaction chamber.

Two of the three components that are present are well characterized: (i) the first spectrum in the series that corresponds to the fully oxidized Co^{2+} species incorporated in tetrahedral

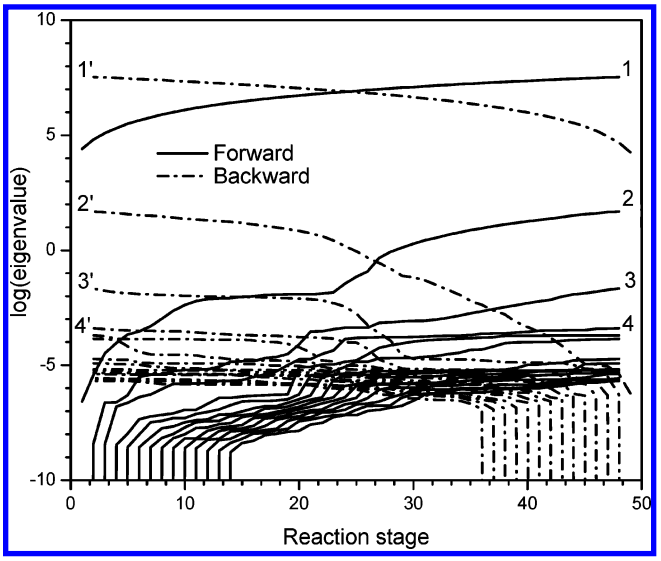

Figure 6. The EFA diagram for the data set in Figure 5: lines are for the forward (solid) and backward (dotted) analyses.

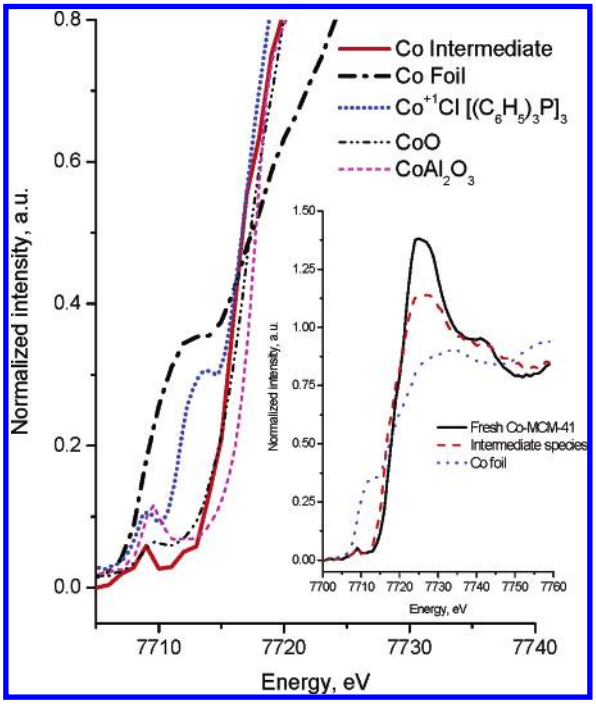

Figure 7. XANES spectra of the intermediate cobalt species formed during catalyst reduction and of reference samples: cobalt foil, chlorotris (triphenylphosphine) cobalt(I) (T_d local Co symmetry), cobalt-(II) oxide (O_h local Co symmetry), cobalt(II) aluminate (T_d local Co symmetry). Inset shows spectra of the three cobalt species identified by EFA in the data set in Figure 5.

sites of the silica framework of the MCM-41 molecular sieve and (ii) the characteristic spectrum of the fully reduced Co^0 species corresponding to the Co nanoparticles detected by EXAFS.[15] Two spectra corresponding to the initial Co^{2+} species and Co foil were used to calculate the spectrum of the intermediate species. The near-edge region of this spectrum is plotted in Figure 7 along with the spectra of several reference compounds, given for comparison, where cobalt is in oxidation states between 2+ and 0. In the inset of Figure 7, the spectrum of the intermediate species is compared to those of the fresh sample and of the cobalt foil. This was carried out to determine the oxidation state and the local coordination of the intermediate species by comparing its XANES spectrum with those of

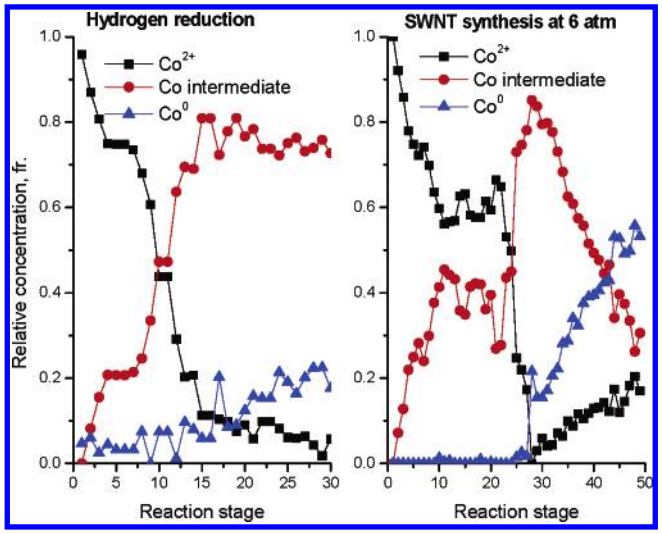

Figure 8. Concentration profiles for the cobalt species formed in the Co−MCM-41 catalyst during reduction in H_2 (left panel) or during SWNT synthesis at 6 atm CO (right panel) as determined from the EFA.

reference compounds with known cobalt oxidation state and local symmetry. The spectral analysis was also performed by using iterative transformation factor analysis (ITFA); this applies the constraint of nonnegativity to the X-ray absorbance and concentration profiles to obtain a transformation matrix, which yields the XANES spectra of the chemical species without using the help of external references.[29] Both methods of calculation give similar XANES spectra for the Co intermediate species.

The spectrum of the intermediary species obtained from the EFA applied to the data set in Figure 5 was further used in linear combinations with the spectrum of the cobalt foil to reconstitute the spectra in the data sets from Figures 1 and 5 and to derive the corresponding concentration profiles plotted in Figure 8. In the case of solid-state materials, it is not sufficient to consider only the electronic state of the metal or oxide species of interest to perform an accurate linear combination analysis, and special attention should be paid to different structural parameters, such as the size and morphology of the clusters, and interatomic distances.[30,31] Since complementary microscopy or X-ray diffraction data with respect to the size and the shape of the cobalt clusters in our samples was impossible to obtain because of their extremely small size,[12] we could not take these factors into consideration. However, the error induced by neglecting these factors in the case of our data treatment cannot significantly affect the evolution of the cobalt species observed in our samples, but their consideration would certainly improve the accuracy.

The diameter distribution of SWNT produced in Co−MCM-41 catalysts was observed to correlate with the size distribution of the metallic clusters initiating the nanotube growth.[11,13,14] We have previously proposed that the particle size distribution depends on the relative rates of cobalt reduction, its nucleation into metallic clusters, and initiation and growth of carbon nanotubes.[15] This is because once a metallic cluster reaches a critical size/energetic state it becomes able to dissociate CO molecules and to precipitate carbon at the surface, which stops its growth and limits its surface mobility. We have previously demonstrated that at lower pressures the SWNT synthesis process is in a kinetically controlled regime with respect to CO.[14] To show how CO pressure affects the dynamics of the cobalt species in the Co−MCM-41 catalyst, and thus the Co cluster growth, we used the EFA technique to analyze the behavior of

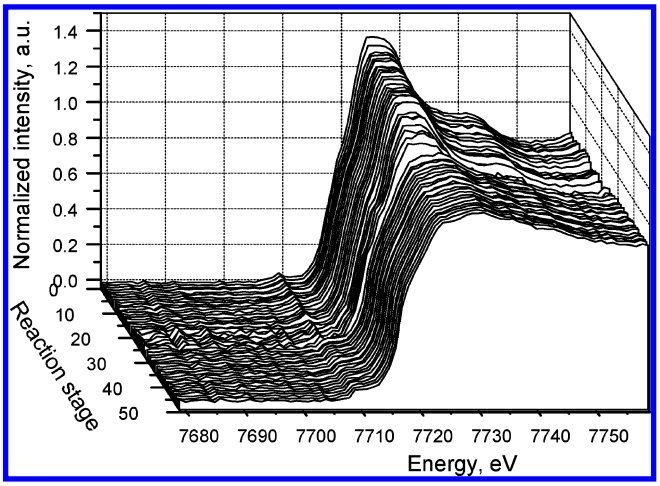

Figure 9. X-ray absorption XANES spectra recorded in situ during catalyst prereduction in H_2 and SWNT synthesis at 750 °C under 2 atm CO pressure.

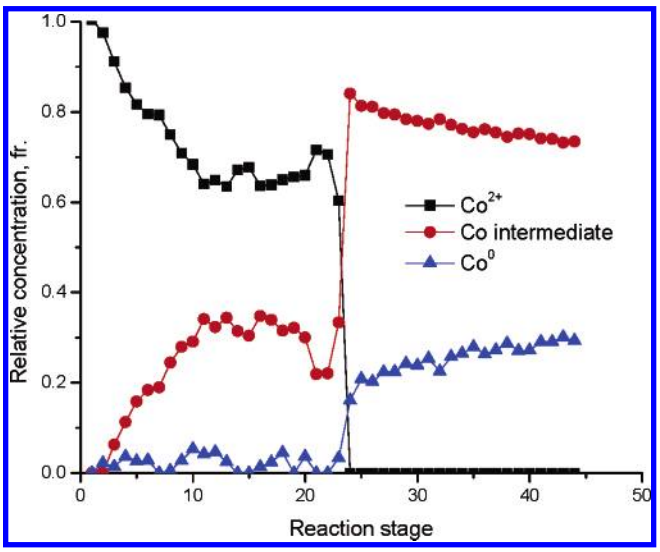

Figure 10. Concentration profiles for the cobalt species formed in the Co−MCM-41 catalyst during SWNT synthesis at 2 atm CO as determined from the EFA.

the Co−MCM-41 at lower CO pressure (2 atm) compared with the previous experiments at 6 atm. The data set in Figure 9 was recorded during an SWNT synthesis experiment similar to the one performed for the data set in Figure 5, but exposing the catalyst to 2 atm CO at 750 °C following an identical prereduction treatment. The EFA diagram (not shown) confirmed the existence of three principal components in the sample, as in the case of the other two data sets, and the resulting concentration profiles are shown in Figure 10. The FTs of the EXAFS spectra recorded at room temperature at the end of the two SWNT synthesis experiments at 2 and 6 atm are given in Figure 11.

Discussion

From the SWNT synthesis perspective, the mechanism of cobalt reduction and formation of metallic clusters is of crucial importance as it has been demonstrated that the size of metallic clusters is a key parameter to control both diameter uniformity and selectivity to SWNT.[11,13−15] Reduction of the Co^{2+} ions isomorphously substituted for silicon ions at tetrahedral sites in the amorphous silica pore wall of the MCM-41 mesoporous

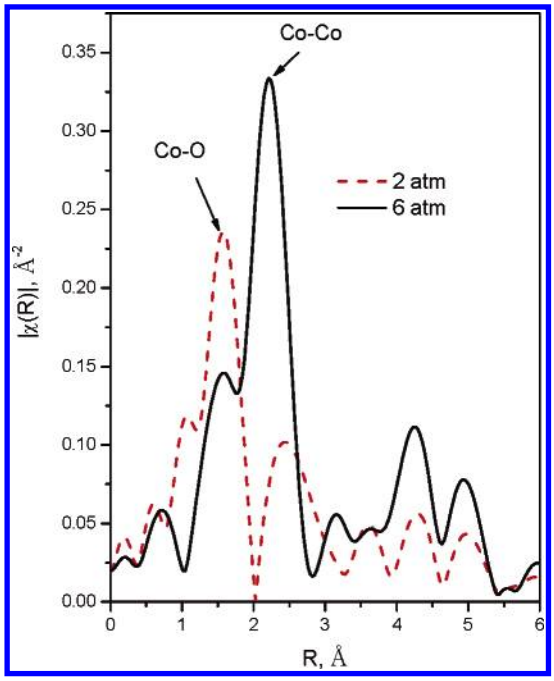

Figure 11. Fourier transforms of EXAFS spectra recorded with the Co−MCM-41 catalysts loaded with carbon after reaction under 2 or 6 atm CO.

molecular sieve is expected to produce significant modifications of the X-ray absorption spectra near the absorption edge. Specifically, the intensity of the white line is expected to decrease as the empty states at the Fermi level are occupied with electrons, the threshold of the absorption edge should shift toward lower energy as the cobalt species becomes more reduced, and the preedge peak is expected to change as the cobalt atoms in the newly formed metallic clusters take on metal properties and assume octahedral environment rather than the tetrahedral one characteristic for the Co^{2+} species in Co-incorporated MCM-41 catalysts. Although the presence of fully reduced metallic Co clusters has been confirmed by the R space EXAFS spectrum recorded with the reduced catalyst, only one of the expected changes in the spectral features is readily observable in the dynamic X-ray absorption spectra in Figure 1 recorded in situ during reduction: the intensity of the white line decreases during reduction, as expected. However, the use of the ProCorA technique enables observation of additional changes in the series of spectra in Figure 1. The peak centered at approximately 7716 eV observed in the synchronous plot constitutes evidence for changes in the position of the threshold of the absorption edge indicative of changes in the oxidation state of the cobalt species. This peak was first observed when the synchronous intensity was calculated with the first three spectra in the series (not shown) and increased in intensity as more spectra were added to the series used to compute the synchronous correlation intensity. Moreover, the negative peak at energy coordinates (7716, 7710) in the asynchronous plot confirms that by starting with the ninth spectrum of the series, there are also changes in the preedge feature of the spectra. ProCorA indicates that the changes in the XAS spectra occurred first in the white line, then in the threshold of the absorption edge starting with the third spectrum, and eventually, a change in the preedge feature was initiated at the ninth spectrum in the series. This sequence is also suggested by the asynchronous plot in Figure 2 as the negative cross-peak at (7716, 7710) has a negative corresponding peak in the synchronous plot suggesting the change at 7716 eV occurs before the change at 7710 eV. This sequence is consistent with that observed previously in a similar experiment.[16]

The change in the preedge peak occurs considerably later than those in the other two features. Such behavior suggests that the reduction of the Co^{2+} species may proceed through some intermediate species rather than a direct reduction to metallic cobalt. While the presence of the two cobalt states, Co^{2+} (characteristic of the Co isomorphously substituted for silicon ions in MCM-41 prior to reduction) and Co^0 (fully reduced metal), is unambiguously evidenced by the two peaks in the R space EXAFS spectrum of the reduced sample given in Figure 3, the EFA diagram in Figure 4 suggests that there is a third chemical species whose spectrum would have to be used in linear combinations to recompose the spectra in the data set in Figure 1. The ideal data set to be used to determine the spectrum of each species present in the sample should contain spectra in which each of the species has a high enough concentration to produce a significant effect in the X-ray absorption spectrum. Because of the low concentration of the metallic species in the data set in Figure 1 suggested by the R space EXAFS spectrum in Figure 3, the data set in Figure 5, in which most of the Co^{2+} species is gradually reduced to metallic cobalt, is more appropriate to identify the spectra of each species. This is also suggested by the EFA diagram in Figure 6 that shows a better separation between the eigenvalues for the significant species (the first three) and those induced by the small normalization errors inherent to this analysis.

The spectrum of the intermediate species given in Figure 7 was determined from the EFA using the spectra of the fresh Co−MCM-41 and of the Co foil for two of the components because these two species are present in the sample during this experiment. The spectrum of the intermediate species resembles the spectrum of the chlorotris (triphenylphosphine) cobalt(I) reference sample in two respects. First, the threshold of the absorption edge is located at about the same energy, between the corresponding values of Co^0 and Co^{2+} reference compounds. Second, the preedge peak is located at the same energy and has approximately the same width, suggesting the local symmetry of the cobalt species in these compounds is similar. The Co^{1+} ion in the $Co(PPh_3)_3Cl$ compound has a local symmetry of C_{3v}.[32] The Co^{1+} intermediate species is thus compatible with the tetrahedrally coordinated (or close subgroup) local environment ascribable to Co ions substituted isomorphously for Si^{4+} in the MCM-41 framework. It is therefore concluded that the reduction of the Co^{2+} ions incorporated into the silica framework of the MCM-41 materials proceeds through an intermediary Co^{1+} like state. These species are most likely still embedded in the pore wall rather than exposed to the surface; therefore, they preserve their tetrahedral coordination.

The concentration profiles given in Figure 8 for each cobalt species were obtained from the data sets in Figures 1 and 5 recorded during the reduction and SWNT synthesis experiments, respectively. In both samples, the metallic cobalt starts to form only after most of the Co^{2+} ions were reduced to the intermediary species. There is, however, a significant difference between the dynamics of the reduction processes in the two samples: the reduction of the intermediate species to metallic cobalt proceeds considerably faster under CO atmosphere than under H_2.

The prereduction in H_2 at 500 °C for 30 min creates exclusively intermediate cobalt species. On heating the sample under flowing He to 750 °C, there is no visible change in the concentration profiles, suggesting the cobalt does not get further reduced. However, on exposure to 6 atm CO at 750 °C, there

is a rapid reduction of the Co^{2+} ions to the intermediate species, followed by a rapid conversion of the intermediate into metallic cobalt. The steep increase in the reduction rate upon exposure to CO is also accompanied by the formation of the first metallic species in this sample. These differences in the behavior of the cobalt species under the two different experimental conditions is most likely due to the differences between the chemical nature of the interactions between the cobalt intermediate and H_2 and CO, respectively. While H_2 is very effective in producing the intermediate cobalt species, the CO is more effective in completely reducing the intermediate species to the metal.

In our previous work, we have observed that a catalyst heated to the reaction temperature (750 °C) in He and subsequently exposed to CO was reduced only to a very low extent and have suggested the CO does not have access to the Co ions buried in the silica pore wall, and that prereduction in hydrogen is required to make the cobalt accessible to the CO molecules.[15] The results presented here confirm that prereduction in H_2 is required for the formation of metallic Co clusters for SWNT growth in the presence of CO. However, recent experiments with Ni incorporated MCM-41 have demonstrated that for this catalyst hydrogen prereduction is not required to fully reduce the Ni in CO at 750 °C.[33] Since the pore wall structure of Co−MCM-41 is expected to be similar to that of the Ni−MCM-41, this result suggests that it is not a diffusional barrier that impedes the reduction of cobalt by CO, but the interaction between the Co^{2+} ions and CO molecules, which is believed to be weaker than that occurring between Ni ions and CO. Similarly, it is likely that the intermediate Co^{1+} like compound which is still strongly bound in the silica framework interacts stronger with the CO molecules, similar to the Ni^{2+} ions in Ni−MCM-41, and the hydrogen prereduction is only required to create the CO-reactive Co^{1+} species. It is therefore proposed that nucleation of the cobalt clusters proceeds via a cobalt carbonyl-like compound obtained after interaction of the Co^{1+} species with one or more CO molecules. As soon as the cluster size reaches a critical size or electronic state, the SWNT growth is initiated, the cluster is immobilized by the carbon nanotube, and its growth ceases. This provides a more complete picture of the mechanism proposed before and demonstrates that the reduction process can be finely tuned to control the size of the metallic clusters formed in Co−MCM-41. However, it is likely that this mechanism will not work for every transition-metal ion, as we have shown it does not work for Ni because the reduction of Ni is thermodynamically more favorable than cobalt.[6]

A rather intriguing observation is that, after the Co^{2+} ions are completely converted into the intermediate species, their concentration starts to increase again showing that some Co^{2+} species are present in the sample at the end of the experiment (Figure 8). The FTs in Figure 11 recorded for this sample at the end of the experiment show a small Co−O peak characteristic for the Co^{2+} species, but the presence of the intermediate species in the sample could generate a peak near or at the same location as they essentially maintain the local geometry of the Co ions in the calcined material. A reoxidation of the intermediate species, however, is not clearly inferred from the data, and we propose that this unexpected behavior is most likely due to the errors induced by the less precise normalization procedure we were forced to apply to be able to use the EFA with these data sets. Therefore, quantitative assessments based on these data are not justified. It is possible, however, that oxidized cobalt species result from the formation of surface carbide on the few larger cobalt particles formed in the catalyst. Formation of such carbide compounds has been observed in related experiments performed under similar conditions.

The separate SWNT synthesis experiment performed using identical prereduction conditions, but using only 2 atm CO during the SWNT growth, was used to test the consistency of this analysis. When analyzed by EFA using the same spectra for the cobalt species in the sample as with the other two data sets, the series of spectra in Figure 9 produced the concentration profiles in Figure 10. First, it should be noted that the concentration profiles recorded during catalyst prereduction and heating in He to 750 °C (reaction stage below 24) mirror those observed with the previous SWNT synthesis experiment, with the slight differences in concentration most likely because of spectra normalization procedure and the uncertainties introduced by the linear combination procedure, as discussed above. Second, a similar rapid reduction of the Co^{2+} to the intermediate species is observed upon catalyst exposure to CO. However, the complete reduction of the intermediary species to metallic Co is considerably slower, suggesting that the reduction kinetics for the intermediary species to metallic Co is strongly influenced by the CO pressure, consistent also with the R space EXAFS spectrum in Figure 11 recorded for this sample showing a much stronger Co−O peak than that observed for the sample reacted at 6 atm. This is consistent with SWNT growth experiments showing increased SWNT yield at 6 atm compared to 2 atm and postulated to be due to an increased density of the small reduced Co clusters that act as nucleation sites for SWNT growth. It also supports the hypothesis that CO is needed to make the Co species more mobile at the MCM-41 surface.

The significant effect of the CO pressure on the reduction process might be exerted through two different effects; first, the effect on the reduction of Co^{2+} species to the intermediate Co^{1+}, and second, the reduction of the intermediate to the metal. While the CO pressure has little, if any, effect on reduction of Co^{2+} to the intermediate species, it has a pronounced effect on the rate of the complete reduction to the metal of the intermediate species.

Conclusion

Both ProCorA and EFA chemometric techniques have proved useful in the analysis of the in-situ dynamic X-ray absorption spectroscopy data collected during reduction in pure hydrogen and under single-wall carbon nanotubes synthesis reaction conditions with a Co−MCM-41. ProCorA establishes the sequence in which changes in the spectral features near the Co K-edge occurred, and the EFA facilitates the observation of the formation of an intermediate Co^{1+} ionic species during reduction of the Co−MCM-41 catalyst in pure hydrogen up to 720 °C. The intermediate species preserves the tetrahedral coordination inside the silica framework and is resistant to complete reduction to the metal in H_2. However, while the Co^{2+} species is difficult to reduce in pure CO, the intermediate Co^{1+} species is more reactive in the presence of CO, presumably by forming Co carbonyl−like compounds with high mobility. Binding CO molecules may weaken the interaction of the Co^{1+} species with the surrounding oxygen ions from the MCM-41 silica matrix, so that they can nucleate into clusters. These clusters grow in size until they reach the size and electronic state required to initiate the growth of carbon nanotubes. After SWNT growth initiation, the clusters are immobilized by the attached carbon nanotubes, and their growth is impeded by the covering carbon layer at their surface. Controlling the rates of each step of this two-stage reduction process is likely the key to controlling the size of the metallic Co clusters formed in Co−MCM-41 catalysts.

Acknowledgment. We thank the Department of Energy, Office for Basic Energy Sciences for funding and the National Synchrotron Light Source, Brookhaven National Laboratory for the X-ray absorption spectroscopy experiments.

References and Notes

(1) Corma, A.; Garcia, H. *Chem. Rev.* **2002**, *102*, 3837.

(2) Johnson, B. F. G.; Raynor, S. A.; Brown, D. B.; Shephard, D. S.; Mashmeyer, T.; Thomas, J. M.; Hermans, S.; Raja, R.; Sankar, G. *J. Mol. Catal. A: Chem.* **2002**, *182*, 89.

(3) Imperor-Clerc, M.; Bazin, D.; Appay, M. D.; Beaunier, P.; Davidson, A. *Chem. Mater.* **2004**, *16*, 1813.

(4) Lim, S.; Ciuparu, D.; Pak, C.; Dobek, F.; Chen, Y.; Harding, D.; Pfefferle, L.; Haller, G. L. *J. Phys. Chem. B* **2003**, *107*, 11048.

(5) Vralstad, T.; Oye, G.; Ronning, M.; Glomm, W. R.; Stocker, M.; Sjoblom, J. *Microporous Mesoporous Mater.* **2005**, *80*, 291.

(6) Yang, Y.; Lim, S.; Du, G.; Chen, Y.; Ciuparu, D.; Haller, G. L. *J. Phys. Chem.* **2005**, *109*, 13237.

(7) Amama, P. B.; Lim, S.; Ciuparu, D.; Yang, Y.; Pfefferle, L.; Haller, G. L. *J. Phys. Chem. B* **2005**, *109*, 2645.

(8) Pak, C.; Haller, G. L. *Stud. Surf. Sci. Catal.* **2001**, *135*, 1004.

(9) Sobczak, I.; Ziolek, M.; Renn, M.; Decyk, P.; Nowak, I.; Daturi, M.; Lavalley, J.-C. *Microporous Mesoporous Mater.* **2004**, *74*, 23.

(10) Mulukutla, R. S.; Shido, T.; Asakura, K.; Kogure, T.; Iwasawa, Y. *Appl. Catal., A* **2002**, *228*, 305.

(11) Ciuparu, D.; Chen, Y.; Lim, S.; Haller, G. L.; Pfefferle, L. *J. Phys. Chem. B* **2004**, *108*, 503.

(12) Lim, S.; Ciuparu, D.; Chen, Y.; Yang, Y.; Pfefferle, L.; Haller, G. L. *J. Phys. Chem. B* **2005**, *109*, 2285.

(13) Chen, Y.; Ciuparu, D.; Lim, S.; Yang, Y.; Haller, G. L.; Pfefferle, L. *J. Catal.* **2004**, *225*, 453.

(14) Chen, Y.; Ciuparu, D.; Lim, S.; Yang, Y.; Haller, G. L.; Pfefferle, L. *J. Catal.* **2004**, *226*, 351.

(15) Ciuparu, D.; Chen, Y.; Lim, S.; Yang, Y.; Haller, G. L.; Pfefferle, L. *J. Phys. Chem. B* **2004**, *108*, 15565.

(16) Haider, P.; Chen, Y.; Lim, S.; Haller, G. L.; Pfefferle, L.; Ciuparu, D. *J. Am. Chem. Soc.* **2005**, *127*, 1906.

(17) Lim, S.; Yang, Y.; Ciuparu, D.; Wang, C.; Chen, Y.; Pfefferle, L.; Haller, G. *Top. Catal.* **2005**, *34*, 31.

(18) Barrett, E. P.; Joyner, L. G.; Halenda, P. P. *J. Am. Chem. Soc.* **1951**, *73*, 373.

(19) Stern, E. A.; Newville, M.; Ravel, B.; Yacoby, Y.; Haskel, D. *Physica B* **1995**, *209*, 117.

(20) Ankudinov, A. L.; Ravel, B.; Rehr, J. J.; Conradson, S. D. *Phys. Rev. B* **1998**, *58*, 7565.

(21) Noda, I.; Dowrey, A. E.; Marcott, C.; Story, G. M.; Ozaki, Y. *Appl. Spectrosc.* **2000**, *54*, 236a.

(22) Haider, P.; Haller, G. L.; Pfefferle, L.; Ciuparu, D. *Appl. Spectrosc.* **2005**, *59*, 53.

(23) Noda, I. *Appl. Spectrosc.* **1993**, *47*, 1329.

(24) Bazin, D. C.; Sayers, D. A.; Rehr, J. J. *J. Phys. Chem. B* **1997**, *101*, 11040.

(25) Malinowski, E. R. *Factor Analysis in Chemistry*, 3rd ed.; Wiley: New York, 2002.

(26) Wang, X. Q.; Hanson, J. C.; Frenkel, A. I.; Kim, J. Y.; Rodriguez, J. A. *J. Phys. Chem. B* **2004**, *108*, 13667.

(27) Marquez-Alvarez, C.; Rodriguez-Ramos, I.; Guerrero-Ruiz, A.; Haller, G. L.; Fernandez-Garcia, M. *J. Am. Chem. Soc.* **1997**, *119*, 2905.

(28) Gampp, H.; Maeder, M.; Meyer, C. J.; Zuberbuhler, A. D. *Talanta* **1986**, *33*, 943.

(29) Fernandez-Garcia, M.; Alvarez, C. M.; Haller, G. L. *J. Phys. Chem.* **1995**, *99*, 12565.

(30) Bazin, D.; Rehr, J. J. *J. Phys. Chem. B* **2003**, *107*, 12398.

(31) Fernandez-Garcia, M.; Martinez-Arias, A.; Hanson, J. C.; Rodriguez, J. A. *Chem. Rev.* **2004**, *104*, 4063.

(32) Edwards, H. G. M.; Lewis, I. R.; Turner, P. H. *Inorg. Chim. Acta* **1994**, *216*, 191.

(33) Chen, Y.; Ciuparu, D.; Yang, Y.; Lim, S.; Wang, C.; Haller, G. L.; Pfefferle, L. *Nanotechnology* **2005**, *16*, S476.